NAVAL POSTGRADUATE SCHOOL

Monterey, California

THESIS

SUBSCALE SOLID ROCKET MOTOR
INFRARED SIGNATURE AND
PARTICLE BEHAVIOR

by

John A. Racine

December, 1991

Thesis Advisor: David W. Netzer

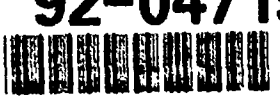

REPORT DOCUMENTATION PAGE

1a. REPORT SECURITY CLASSIFICATION Unclassified	1b. RESTRICTIVE MARKINGS
2a. SECURITY CLASSIFICATION AUTHORITY	3. DISTRIBUTION/ AVAILABILITY OF REPORT Approved for public release; distribution is unlimited.
2b. DCLASSIFICATION/DOWNGRADING SCHEDULE	
4. PERFORMING ORGANIZATION REPORT NUMBER(S)	5. MONITORING ORGANIZATION REPORT NUMBER(S)
6a. NAME OF PERFORMING ORGANIZATION Naval Postgraduate School 6b. OFFICE SYMBOL *(If Applicable)*	7a. NAME OF MONITORING ORGANIZATION Naval Postgraduate School
6c. ADDRESS *(city, state, and ZIP code)* Monterey, CA 93943-5000	7b. ADDRESS *(city, state, and ZIP code)* Monterey, CA 93943-5000
8a. NAME OF FUNDING/SPONSORING ORGANIZATION AIR FORCE PHILLIPS LABORATORY 6b. OFFICE SYMBOL *(If Applicable)*	9. PROCUREMENT INSTRUMENT IDENTIFICATION NUMBER
8c. ADDRESS *(city, state, and ZIP code)* Edwards Air Force Base, California	10. SOURCE OF FUNDING NUMBERS PROGRAM ELEMENT NO. / PROJECT NO.F04611-91-X-0004 / TASK NO. / WORK UNIT ACCESSION NO.

11. TITLE *(Include Security Classification)*
SUBSCALE SOLID ROCKET MOTOR INFRARED SIGNATURE AND PARTICLE BEHAVIOR

12. PERSONAL AUTHOR(S)
Racine, John A.

13a. TYPE OF REPORT	13b. TIME COVERED FROM TO	14. DATE OF REPORT *(year, month,day)*	15. PAGE COUNT
Master's Thesis		December, 1991	54

16. SUPPLEMENTARY NOTATION
The views expressed in this thesis are those of the author and do not reflect the official policy or position of the Department of Defense or the U.S. Government.

17. COSATI CODES			18. SUBJECT TERMS *(continue on reverse if necessary and identify by block number)*
FIELD	GROUP	SUBGROUP	Solid Propellant Collection Probe Particle Size Distribution

19. ABSTRACT *(Continue on reverse if necessary and identify by block number)*

A combined optical and particle collection probe which employed an in situ particle size distribution measurement method and an infrared camera were used to obtain data that could be used to validate solid propellant rocket motor plume signature prediction codes. The probe design was optimized and the required rates for window purge and ejector flows were determined which provided proper functioning of the probe when place in the supersonic region of the plume. At the nozzle exit the particle size distribution was quadramodal with most particles smaller than 0.5μ and the largest particles with diameters less than 25μ. The larger particles at the nozzle exhaust were not present further aft in the plume. This behavior was believed to result from the breakup of the large Al_2O_3 particles in the plume Mach discs. However, further work is required to determine if the probe alters the particle size distribution.

20. DISTRIBUTION/AVAILABILITY OF ABSTRACT	21. ABSTRACT SECURITY CLASSIFICATION
[X] UNCLASSIFIED/UNLIMITED [ ] SAME AS RPT. [ ] DTIC USERS	Unclassified
22a. NAME OF RESPONSIBLE INDIVIDUAL David W. Netzer	22b. TELEPHONE (Include Area Code) (408) 646-2980 / 22c. OFFICE SYMBOL AA/Nt

DD FORM 1473, 84 MAR 83 APR edition may be used until exhausted SECURITY CLASSIFICATION OF THIS PAGE
All other editions are obsolete Unclassified

Approved for public release; distribution is unlimited.

Subscale Solid Rocket Motor Infrared Signature
and Particle Behavior

by

John A. Racine
Lieutenant, United States Navy
B.A., Huntingdon College, 1985

Submitted in partial fulfillment
of the requirements for the degree of

MASTER OF SCIENCE IN ASTRONAUTICAL ENGINEERING

from the

NAVAL POSTGRADUATE SCHOOL
December 1991

Author: 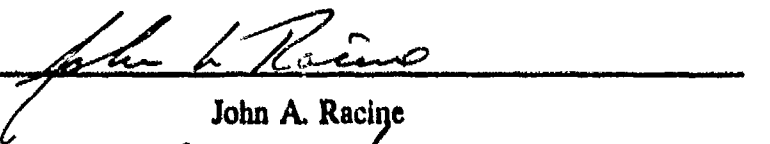

John A. Racine

Approved by: 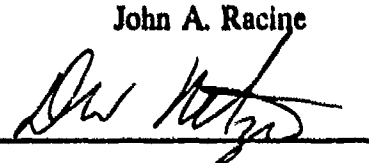

D.W. Netzer, Thesis Advisor

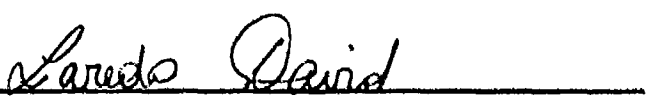

David Laredo, Second Reader

D.J. Collins, Chairman
Department of Aeronautics and Astronautics

ABSTRACT

A combined optical and particle collection probe which employed an in situ particle size distribution measurement method and an infrared camera were used to obtain data that could be used to validate solid propellant rocket motor plume signature prediction codes. The probe design was optimized and the required rates for window purge and ejector flows were determined which provided proper functioning of the probe when placed in the supersonic region of the plume. At the nozzle exit the particle size distribution was quadramodal with most particles smaller than 0.5μ and the largest particles with diameters less than 25μ. The larger particles at the nozzle exhaust were not present further aft in the plume. This behavior was believed to result from breakup of the large Al_2O_3 particles in the plume Mach discs. However, further work is required to determine if the probe alters the particle size distribution.

TABLE OF CONTENTS

LIST OF TABLES

LIST OF FIGURES

I. INTRODUCTION

The characteristics of exhaust products of solid propellant rocket motors (SRM's) continue to be of major importance to SRM system designers. Predictions from commonly used plume codes such as the JANNAF Standard Plume Flowfield Model (SPF) and the Standardized Infrared Radiation Model (SIRRM [Ref. 1,2]) are sensitive to the particle size distribution [Ref. 3] and optical properties. Errors in the plume particle size distribution calculated with SPF cascade into the plume radiation prediction from SIRRM. Experimental validation of such codes has not been accomplished to an acceptable degree. In addition, the sensitivity of the model predictions to the specified input data needs to be determined in order to know how accurately experimental data must be obtained in code validation efforts. Because of the severity of the motor and plume environments very little data exist which can be used to validate the code predictions for the particulate behavior within the exhaust nozzle or plume.

Several different methods have been utilized to study particle size distributions in motors and plumes. These include:

1. transmitted light measurements [Ref. 4],
2. scattered light measurements [Refs. 5,6,7] and

3. particle collection [Refs. 5,6].

The problems associated with these methods are numerous. Measurements through the plumes of even moderately aluminized propellants are quite difficult due to multiple light scattering and beam extinction. For these reasons a combined optical and particle collection probe [Refs. 5,6] was used to isolate a small streamtube of the plume for optical measurement. The probe initially designed by Eno [Ref. 5] and modified by Kellman [Ref. 6] was designed to overcome four basic problems encountered in the collection and measurement of exhaust products in plumes [Ref 5]:

1. Bias of the sample from disturbances to the flow in the streamtube to be captured;

2. Particle entrainment effects from the atmosphere which can introduce foreign particles into the sample;

3. Breakup or agglomerates during collection and subsequent handling; and

4. Continued chemical reaction of the particles.

Initial use of the probe was only partially successful due to contamination of the optical windows. Also, one set of probe operating conditions was not found adequate for all probe locations within the plume.

This investigation attempted to overcome these initial problems by:

1. redesigning the probe interior flowfield to reduce flow recirculation,

2. optimizing the probe ejector and window purge flow rates and pressures, and

3. optimizing the probe sampling time.

In addition it was desired to determine under what conditions/plume locations, the probe would not provide reliable data. After probe validation efforts were completed it was desired to use the probe to measure the changes in particle size distribution along the plume centerline. These data are needed for validation of the SPF code predictions. Infrared (IR) camera images were also taken to provide data which can be used to correlate with the measured particle size distributions, and with the code predictions for plume radiation.

II. EXPERIMENTAL APPARATUS

A. BACKGROUND

A three dimensional subscale rocket motor, a exhaust plume deflection device, MALVERN Mastersizer and 2600HSD particle sizing devices, a combined optical measurement and particle collection probe, a Mastersizer protection enclosure and probe mount, an AGEMA IR camera and a PC based data acquisition and control system comprised the equipment required to conduct the tests.

B. EQUIPMENT

1. Three Dimensional Subscale Motor

The solid propellant rocket motor used in this investigation was a simplified version of the one used by Pruitt, et al.[Ref. 7], and by Eno[Ref. 5] and Kellman[Ref. 6]. The motor internal diameter was 2.0 inches and it was 10 inches in length (Figure 2.1). Two propellant grain configurations were used. The first was an end-burning cylinder, 2.0 inches in diameter and 1.00 - 1.25 inches thick. The second, was a centrally-perforated cylinder, 2.0 inches in outside diameter and a 1.4 inches inside diameter. This radially-burning grain had a length of 1.00 inch. All preliminary runs made to optimize probe ejector and window purge flow rates were conducted using the end-burning grains.

These tests utilized GAP/AP propellants which had small amounts of aluminum (see Table I) and relatively high burning rates. Tests for obtaining plume particle size distributions were conducted using radially-burning grains. In this case a highly aluminized HTPB/AP propellant with a lower burning rate was used (see Table I). The nozzle throat diameter for the motor was sized based on the burning characteristics of the propellants and the desired chamber pressure within the motor. The propellants were bonded to the motor casing using a self vulcanizing silicone rubber compound (RTV). The weight of the propellant was approximately 85 grams for the end-burning grains and 44 grams for the radially-burning grains.

Ignition of the propellant was accomplished by using a small $BKNO_3$ igniter. Igniter initiation utilized a nichrome wire filament energized by a 12 volt power supply.

2. Plume Deflection Device

The plume deflection device served two purposes. First, the volatile environment of the exhaust plume damaged the probe and the Mastersizer. To prevent severe probe damage, the exposure time had to be limited to less than 0.70 seconds. The second purpose of the deflection device was to delay the probe measurement until the motor was operating at the desired steady-state conditions. This also prevented any collection of ignition products. The plume deflection device was the same as that used by Kellman [Ref. 6] and was

fabricated from steel plate. It was actuated via an air pressurized pneumatic piston and valve, which was triggered by a 110 volt solenoid.

3. MALVERN Mastersizer

The MALVERN Mastersizer [Ref. 8] used in conjunction with the probe was the same as that used by Eno [Ref. 5] and Kellman [Ref.6]. It is a commercially produced system utilizing forward scattering of an incident collimated laser beam to determine particle size distribution.

The Mastersizer uses a 2mW helium-neon (He-Ne) laser (633 nanometers wavelength), with a beam diameter of 18 millimeters (mm). The laser and receiver units are self-supporting and mounted on an integrated optical bench which allows for the use of various sample presentation cells and accessories.

The receiver unit has three lens options with focal lengths of 45, 100, and 300 mm. For this investigation the 100 mm collecting lens was used for motor firing experiments and data collection. The 100 mm lens is used as a Fourier transform lens and can measure particles with diameters in the range of 0.48 - 170 microns. The dynamic range of each lens is 800:1 and the accuracy claimed for the system is +/- 2% for a volume median diameter [Ref. 8].

The Mastersizer utilizes a 31 element solid state detector consisting of 31 individual chips mounted in a single

pie-shaped array. The Mastersizer software allows for the sampling of all 31 detectors in 12 milliseconds (ms), termed a sweep. The system allows for multiple sweeps to be averaged and used for the calculation of the particle size distribution. In the present investigation thirty sweeps were initially used. However, to reduce probe window exposure time, later tests utilized only fifteen sweeps.

Various values of differential refractive index and absorptive index of the measured media can be taken from a table in the instruction manual and input into the Mastersizer software. The appropriate values are determined by the user based on the anticipated particle and gas compositions. The forward scattering is measured to an angle of approximately 50°. The software allows for Mie corrections to the Fraunhoffer diffraction theory, permitting particles in gas with diameters as small as 0.5 microns to be measured. The system is capable of measuring multimodal distributions.

4. MALVERN 2600HSD Particle Sizer

This particle sizer [Ref. 9] is similar to the Mastersizer but is based solely on Fraunhofer diffraction. Scattered light is measured to a maximum of 14°. With the 100 mm collecting lens the measured particle size range is 1.91-180 microns. This device employs a 9 mm diameter He-Ne laser beam and was used to measure the particle size distribution

across the entire plume, at a distance as close as possible to the nozzle exit plane.

5. Particle Collection Probe

The particle collection probe shown in (Figure 2.2) is a modification of the probe originally designed by Eno [Ref. 5] and previously modified by Kellman [Ref. 6]. The original probe (Figure 2.3) was designed to use some of the features of the large AFRPL collection probe. The probe was used in conjunction with the Mastersizer to obtain in situ particle size distribution measurements of the particles in the exhaust plume of a solid propellant rocket motor. It captures a small streamtube (0.2 inch diameter) of the exhaust plume to allow the Mastersizer to measure a particle distribution, while minimizing disturbances to the captured flow. This was accomplished by the probe tip being designed so that its external cone angle, ejector flow and back pressure prevented the formation of any bow shock (normal detached shock) for flow Mach numbers greater than approximately 1.4 (Figure 2.4). The flow inside the probe was viewed through two windows. The first was circular, large enough to allow passage of the 18 mm diameter laser beam. The second was a much larger rectangular window to allow forward scattered light angles up to 50°. The windows were kept clean by simultaneously using two methods. The first was by injecting an annular flow of dry nitrogen around the particle laden streamtube to restrict the expansion

of the streamtube to the windows. The second method used dry nitrogen injection very close and parallel to the window surfaces, providing a buffer zone to prevent particles from collecting on the windows.

The primary modification made to the probe was to place the tip at the center of the body to reduce the internal flow recirculation that was present in the initial design.

6. Experiment Control And Data Acquisition

The complexity and short test time of the firing sequence and data collection required the use of an automated control system. Labtech Notebook is a commercially produced software program which can be tailored to the requirements of the experiment. All aspects of the firing sequence and data collection were controlled by the Labtech Notebook program and an IBM/AT microcomputer.

The chamber pressure was used as the triggering input to the data collection sequence. Chamber pressure was determined utilizing a 0-1000 psi strain-gauge pressure transducer attached to a pressure tap located approximately 1.0 inch upstream of the exhaust nozzle entrance. A typical firing sequence and pressure trace are illustrated in (Figure 2.5) and channel assignments are listed in Table II.

7. Infrared Camera

A brief introduction to the theory of blackbody radiation will help to make clear the fundamental principles of the infrared camera used in this study.

A blackbody is an object which absorbs all radiation that impinges on it at any wavelength. Three expressions are available to describe the radiation emitted by a blackbody; Planck's Law, Wien's Law and the Stefan-Boltzman Law.

a. Planck's Law

The spectral distribution of the radiation from a blackbody is given by Planck's Law:

$$W_{\lambda b} = 2\pi hc^2 / {}^5(e^{hc/\lambda kT} - 1) \times 10^{-6} \text{ [Watts/m}^2\mu\text{m]}$$

where,

- $W_{\lambda b}$ = the blackbody spectral radiant emittance at wavelength λ.
- c = the velocity of light = 2.998×10^8 m/sec
- h = Planck's constant = 6.626×10^{-39} Joule sec
- k = Boltzman's constant = 1.381×10^{-23} Joule/K
- T = the absolute temperature (K) of the blackbody
- λ = wavelength (m)

For any given temperature the spectral emittance is zero at λ=0, then rapidly increases to a maximum at λ_{max} and then approaches zero again at much longer wavelengths. The higher the temperature, the shorter the wavelength at which the maximum occurs.

b. Wien's Displacement Law

By differentiating Planck's law with respect to λ, and finding the maximum, Wien's formula is derived.

$$\lambda_{max} = 2898/T \ (\mu m)$$

This formula mathematically expresses the common observation that colors vary from red to orange to yellow as the temperature of a thermal radiator increases. The wavelength of the color is the same as that calculated for λ_{max}.

c. Stefan-Boltzman Law

By integrating Planck's law from $\lambda = 0$ to $\lambda = \infty$, the total radiant emittance (W_b) of a blackbody can be obtained.

$$W_b = \sigma T^4 \ (Watts/m^2)$$

where,

σ = the Stefan-Boltzman constant = 5.6705×10^{-8} Watts/m^2K^4

This formula states that the total radiant emittance is proportional to the fourth power of the absolute temperature of the radiator. W_b represents the area under the Planck curve for a given temperature.

Real objects almost never act as true blackbody radiators. Therefore, some modification to these laws must be made for them to be valid for so-called "grey" bodies. There are three processes which prevent a real object from acting like a blackbody. These are, partial absorption, α, reflection, ρ, and transmittance, τ. All of these factors are

more-or-less wavelength dependent and are represented as α_λ, ρ_λ, andτ_λ, respectively. The sum of these three factors must add to unity at any wavelength. Therefore,

$$\alpha_\lambda + \rho_\lambda + \tau_\lambda = 1$$

Another factor, emissivity, ε, is required to fully describe the fraction of radiant emittance of a blackbody produced at a specific temperature which is emitted by a grey body. Expressed mathematically, the spectral emissivity can be written as such:

$$\varepsilon_\lambda = W_{\lambda o}/W_{\lambda b}$$

where,

- $W_{\lambda o}$ = the spectral radiant emittance of the object being compared to a blackbody at the same temperature.

For a blackbody, $\varepsilon = 1$ and for a grey body $\varepsilon < 1$. Taking into account the emissivity of a grey body, the Stefan-Boltzman law becomes

$$W = \varepsilon \sigma T^4 \text{ (Watts/m}^2\text{)}.$$

This shows that the spectral radiance of a grey body is the same as that of a blackbody at the specified temperature, reduced in proportion to the emissivity, ε, of the grey body.

d. Camera Specifications

The IR scanner unit used was an AGEMA Thermovision 870. This unit converts electromagnetic thermal energy radiated from an object within the field of view into an electronic video signal which can be displayed on a COMPAQ TIC 2000 computer.

The most critical part of the scanner unit is the detector. The detector is entitled SPRITE - Signal PRocessing In The Element. This is actually an infrared sensitive material (mercury cadmium telluride) mounted on a sapphire substrate. The SPRITE detector operates at a temperature of -70 C. This is accomplished using a 3-stage thermoelectric cooler.The detector is sensitive in the 2 - 5 micron range.

The scanner unit of the Thermovision 870 can be fitted with one of five lenses. For this study a 20° field of view lens was used, with the detector placed approximately 2 m from the SRM exhaust plume region under investigation. A glass filter was also used to prevent detector saturation.

III. EXPERIMENTAL PROCEDURE

A. PROBE VALIDATION

Prior to using the probe for actual data collection several motor firings were conducted to determine

1) if the ejector flow and window purge flow rates and pressures were capable of keeping the optical windows clean of exhaust products, and

2) at which locations the probe would not yield reliable data.

1. Determination Of Optimum Window Purge

This process involved several firings of the subscale motor. A GAP/AP propellant containing small amounts of aluminum was used with the probe located at approximately 20 jet diameters downstream of the nozzle exit plane. The window purge and ejector flow rates and pressures were varied and the Mastersizer was used to take background and sample measurements prior to, during, and after the run to determine if the optical windows remained clean.

2. Determination Of Allowable Probe Locations

This process also involved firing of the subscale motor. Again, a GAP/AP propellant with small amounts of aluminum was used. The probe was located in various subsonic and supersonic portions of the exhaust plume. The Mastersizer was again used determine if the optical windows remained clean

and to measure the relative concentration of exhaust products entering the probe.

B. PRE-FIRE PREPARATION

Initial setup of the system for data collection consisted of pressure transducer calibration, Malvern alignment and enclosure, probe mounting, motor assembly and mounting, and plume deflector alignment.

A strain-gauge pressure transducer was calibrated with a dead weight tester, and measured chamber pressure during the run. The tester was loaded from 0 - 1000 psi in increments of 100 psi from 0-200 psi and increments of 200 psi from 200-1000 psi. The output from the transducer was recorded by the Labtech Notebook software. Using the software link to Lotus 123, a linear regression analysis of the data was conducted to calculate a calibration constant for the transducer.

The Malvern device was placed in an enclosure and the collection probe mounted to the center section [Ref. 6]. The optical windows were mounted using flame retardant gasket material and an O-ring to ensure the air tight quality of the probe. The circular window was canted to eliminate reflections which would adversely affect the laser system alignment. A background measurement was taken with the nitrogen flow to the ejector and window purge off to verify system alignment of the laser beam on the detector diodes. After a satisfactory background measurement was taken the gaps

and seams around the probe and the Malvern enclosure were sealed using duct tape and RTV.

The final assembly of the motor was then conducted and the motor mounted at the desired position relative to the probe (distance from the probe and radial location in the plume). The plume flow deflector was then positioned between the motor and the probe, close to the nozzle exit, to allow for complete deflection of the plume when desired. The pressure tap and burst disk were then attached. The burst disk was utilized as a safety precaution to prevent destruction of the motor in the event that the nozzle became plugged during the run. The burst disk was rated at 1000 psi, which was approximately 2.5 times the expected motor pressure.

The computer programs were then loaded, with the data to be recorded in files delineated according to function and run number. Once all preliminary steps were completed, the $BKNO_3$ igniter was installed and connected to the power source. In the control room the video camera and IR imaging system (if utilized) were prepared. After the area was cleared for safety the Labtech Notebook program was initiated and the firing sequence as depicted in (Figure 2.5) was executed. The purge gas was activated upon activation of the program with ignition occurring 3.0 seconds later. The Malvern program was triggered to perform a background measurement, after the activation of the purge gas, but prior to the lowering of the plume deflector. The deflector was triggered to lower, once

the motor pressure reached 100 psi, for either 0.35 or 0.70 seconds, at which time it would raise again to the deflection position. The Malvern was triggered to take a sample measurement for 0.15 or 0.30 seconds after the deflector lowered and again after the deflector raised back into the deflection position. The latter was done to determine the cleanliness of the windows.

IV. RESULTS AND DISCUSSION

A. EXPERIMENTAL RESULTS

1. Window Purge Rate Optimization

The window purge investigation was carried out simultaneously with probe location studies. A total of eleven motor firings were conducted. Nine of the firings were conducted using a GAP/AP propellant containing 2% aluminum. The remaining two firings were conducted using a GAP/AP propellant with 4.69% aluminum.

The firings made with the 2% Al propellant were conducted with the probe located along the centerline and approximately 22 exit diameters downstream of the nozzle exit plane in the subsonic region of the plume. The runs made with the 4.69% Al propellant were made at the same axial location and approximately 1.0 inch below the plume centerline. These latter runs were made in conjunction with a related investigation [Ref. 4].

The data acquisition system was set to trigger the plume deflection device at a chamber pressure of 100 psia. The Mastersizer was triggered after a delay of 0.3 seconds. The deflection device was repositioned 0.4 seconds later. After a delay of 4 seconds the Mastersizer was internally

triggered to take a final sample measurement with the purge gas on and no exhaust flow.

After completion of a run, the probe was removed and the windows were examined. During these initial tests a significant amount of material was deposited on both windows. Small recirculation zones were also present, located at the upper and lower front corners of the probe. To minimize these effects the optimum pressures at the nitrogen manifold, for the ejector and window purges, were determined to be 160 and 400 psia, respectively.

The Mastersizer measurements showed that the transmittance values through the probe were very high. This was determined to occur for two reasons. First, the probe tip was designed to operate in the supersonic region of the exhaust plume, but the measurements were taken in the subsonic region. The exhaust flow sensed the downstream obstruction and flowed around the probe tip rather than into it. Secondly, the ejector mass flow rate necessary to pull the exhaust flow into the probe tip while the probe was in the subsonic region of the plume diluted the sample streamtube below acceptable levels for reliable measurement.

Two of the runs produced high chamber pressures, greater than 600 psia. This was due to improper bonding of the grain to the motor walls. However, this higher pressure resulted in the probe being located in the supersonic region of the plume. With the purge gas flow rates and pressures set

at the optimum levels (and with the probe exposure time equal to 0.70 seconds) the windows remained cleaner than when the probe was in the subsonic region. For these tests at higher pressures the laser beam obscuration was greater than 70%. It is desirable to have the obscuration less than 50% to limit multiple scattering effects. However, with 70% obscuration the error in D_{32} is approximately only 10% [Ref. 11].

By analyzing the Mastersizer results it was determined that the windows were fouling after the data were taken. This was apparently due to the condensation of HCl/H_2O vapor (for DD1 and DD5) on the windows, trapping particles which remained in the probe. To overcome this problem the time which the probe was exposed to the exhaust flow was reduced to 0.35 seconds, with only a 0.15 second delay between deflector actuation and Mastersizer triggering. The number of sweeps averaged for the calculation of the particle size distribution was also reduced to 15 to decrease the possibility of the windows fouling during data acquisition.

2. Plume Particle Data

A total of four tests were conducted to measure particle size distributions within the plume (tests 12-15). All tests were conducted using a HTPB/AP propellant containing 16% Al. Major results are listed in Table III. Figures 4.1-4.12 show particle volume and number size distributions for runs 12-15. Tests 12-14 were conducted utilizing the

Mastersizer and probe assembly and, therefore, measured only those particles in a small streamtube along the axis of the plume. Test 15 used only the Malvern 2600 HSD. The particle size distribution results from this test were applicable to the entire plume cross-sectional area. Table III shows the probe axial locations and 2600 HSD location in nozzle exit diameters.

Runs 12 and 13 were made at the same location of 22 exit diameters to verify the repeatability of the measurements. As can be seen in Table III the Sauter mean diameter was 0.53 μm and 0.51 μm respectively. This was a difference of less than 4%. The bi-modal distributions shown in Figures 4.1 and 4.4 were also very nearly identical. Thus, test-to-test repeatability did not appear to be a problem. Figures 4.2-4.3 and Figures 4.5-4.6 show the percentage of particles in range for the volume and number distributions shown in Figures 4.1 and 4.4. The largest particle size measured was in the 7.01-8.48 μm range and represented less than 0.1% of the total measured volume. The number distributions showed that most of the particles had diameters less than 0.5 μ.

Run 14 was made closer to the motor exhaust at approximately 15 exit diameters downstream of the nozzle exit plane. The largest particle size measured, by volume, was in the 3.95-4.79 μm range, representing less than 0.1% of the total volume measured. D_{32} for this run was 1.09 μm. Figure

4.7 shows that more volume was contained in the larger mode of the bi-modal distribution when located closer to the nozzle exhaust. Figures 4.8 and 4.9 show the percentage of particles in range for the volume and number distributions shown in Figure 4.7.

Run 15 was made utilizing the 2600 HSD located approximately five exit diameters downstream of the nozzle exit plane. Figure 4.10 showed that a quadra-modal distribution was present with peaks at <1.91,3,9, and 19 μm. The two larger modes were not present further aft in the plume. The mode peak at 1 μ further aft also appeared to have shifted to 3 μ. By number, the particle size distribution showed that 99.9% of all particles measured were less than 3.02 μm. D_{32} for run 15 was 1.12 μm. Figures 4.11 and 4.12 show the percentage of particles in range for the volume and number distributions shown in Figure 4.10. Again, as the nozzle exit plane is approached the maximum particle sizes increased in diameter. Although the particle size number distributions showed no particles larger than 4 microns, the volume distribution clearly showed that a small number of larger particles were present.

The data indicates that there were large particles, 7-25 microns in diameter, at the nozzle exit plane. If they existed further aft, they were present in concentrations below the sensitivity of the MALVERN. MICROPEP calculations for the test conditions (Appendix C) showed the equilibrium exhaust

temperature to be higher than the melting point of aluminum oxide (2318K). The larger particles will generally not be in thermal equilibrium with the gas. Thus, they may remain molten further aft in the plume. The decrease in the number of larger particles further aft in the plume could be explained by their breakup through the Mach discs. However, additional tests are required to determine if the probe causes any of the particle breakup.

The magnitude of the Malvern diode signal voltages during data acquisition were approximately ten times higher than those during post-run measurements. This verified that the limited probe exposure and data acquisition times employed were successful in keeping the probe windows clean.

3. IR Signature

Infrared pictures were taken utilizing the AGEMA Thermovision 870 IR camera during run 15 (see Figure 4.13). Figure 4.13 was taken utilizing a glass filter with an aperture setting of one. Assuming a relative plume emissivity of 0.16, plume centerline temperatures exceeded 400° C at 75 exit diameters from the nozzle exhaust. Future tests will be required to utilize additional filtering if the maximum temperatures are to be measured. A future investigation will attempt to relate the IR data to the measured particle size distributions. In addition, the data will be used to validate the plume signature predictions made using SPF and SIRRM.

B. COMPUTER CODE PREDICTIONS

Due to problems encountered with the initial setup of the computer models only a preliminary test case was conducted. This was accomplished with the assistance of Steve Gruniesen of the Air Force Phillips Laboratory. Figures 4.14 and 4.15 show typical output radiation as a function of plume axial position for the propellant with 2% aluminum (DD1) burned in the subscale motor at 600 psia. This type of data can be compared directly with the IR camera data if the appropriate filters are used. Future investigations will examine code output sensitivity to the specified input data.

V. CONCLUSIONS AND RECOMMENDATIONS

The design and operation of a combined optical/collection particle sizing probe was significantly improved during this investigation. Window purge and ejector flow rates, the probe exposure time and the MALVERN sampling time were optimized to the point that reliable and repeatable particle size data could be obtained in the supersonic portion of the plume.

At the nozzle exit the particle size distribution for a 16% aluminized propellant operated at 325 psia was quadramodal. Most of the particles had diameters less than 0.5 μ, but a few particles as large as 25 μ were present. Further aft, in the center of the plume, the distributions were bimodal with no particles larger than approximately 8 μ. The data appeared to indicate that the larger particles were molten in the supersonic region of the plume and were broken up by passing through Mach discs. However, further efforts are required to determine if the probe causes any particle breakup.

It is recommended that a second probe tip be designed for use in the subsonic region of the plume and that it be utilized in conjunction with the Malvern systems to map the entire plume of a subscale rocket motor. It is also suggested that measurements be made at 15 and 22 exit jet diameters

downstream of the nozzle exit plane with another measuring technique. This is needed to determine if the observed particle breakup occurs through the Mach discs or was caused by the particle collection probe. In addition, it is recommended that a comprehensive sensitivity study be conducted using the plume prediction codes to determine to what degree of accuracy experimentally measured particle size distributions must be obtained for input to the codes.

APPENDIX A

TABLES

TABLE I. COMPOSITION OF PROPELLANTS DD1 (AFAL), DD5 (AFAL), AND SHUTTLE PROPELLANT (Morton Thiokol)

DD1	DD5	SHUTTLE PROPELLANT
Aluminum 2.00%	Aluminum 2.00%	Aluminum 16.0%
AP 73.00%	AP 70.31%	AP 70.0%
GAP 14.67%	GAP 14.67%	HTPB 13.8%
HDI 0.845%	HDI 0.845%	Fe_2O_3 0.2%
TEGON 8.49%	TEGON 8.49%	
TEPANOL 0.15%	TEPANOL 0.15%	
Burning rate exponent n= 0.362	Burning rate exponent n= 0.442	Burning rate exponent n= 0.350
r_{250}= 0.437 in/sec	r_{250}= 0.488 in/sec	r_{625}= 0.37 in/sec

TABLE II. LABTECH NOTEBOOK CHANNEL ASSIGNMENTS

CH#	INTERFACE DEVICE	CHANNEL NAME	CHANNEL TYPE	FILE NAME
1			TIME	RTI(RUN#).PRN
2	1:DASH-16	PRESSURE	ANALOG INPUT	RPR(RUN#).PRN
3		1	TIME	
4		2	CALCULATED	
5		3	CALCULATED	
6		4	CALCULATED	
7		5	CALCULATED	
8	0:PIO-12	PURGE	DIGITAL OUT	RPU(RUN#).PRN
9	0:PIO-12	BACKGROUND	DIGITAL OUT	RBA(RUN#).PRN
10	0:PIO-12	IGNITION	DIGITAL OUT	RIG(RUN#).PRN
11	0:PIO-12	SCANNER	DIGITAL OUT	RSC(RUN#).PRN
12	0:PIO-12	DEFLECTOR	DIGITAL OUT	RDE(RUN#).PRN
13	0:PIO-12	MALVERN	DIGITAL OUT	RMA(RUN#).PRN

TABLE III. MOTOR AND PROBE RESULTS

Test Number	P_c PSIA	Measurement Location[1], in exit diameters	% Al	Mean Particle size, D_{32} (μ)
12*	335	22	16	0.53
13*	350	22	16	0.51
14*	315	15	16	1.09
15**	300	5	16	1.12

* Probe measurements

** Across-plume measurements

APPENDIX B

FIGURES

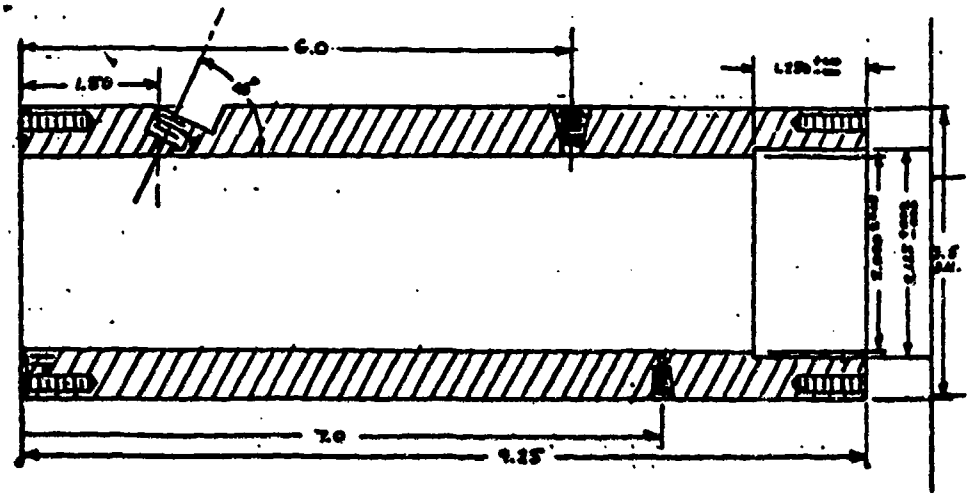

Figure 2.1. Subscale Solid Propellant Rocket Motor

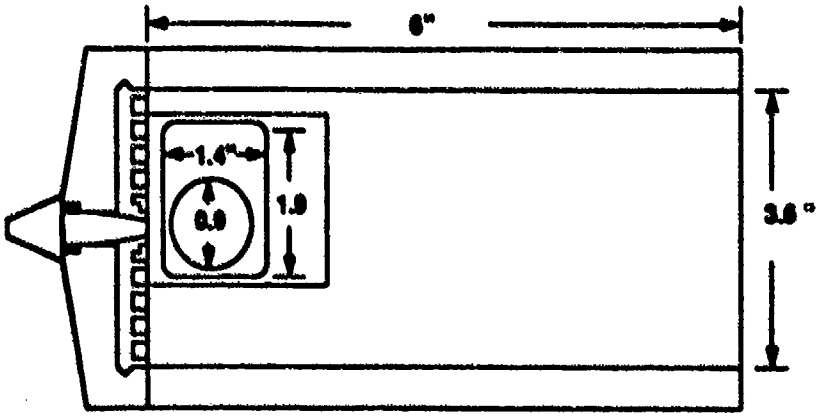

Figure 2.2. Modified Combined Optical and Collection Probe

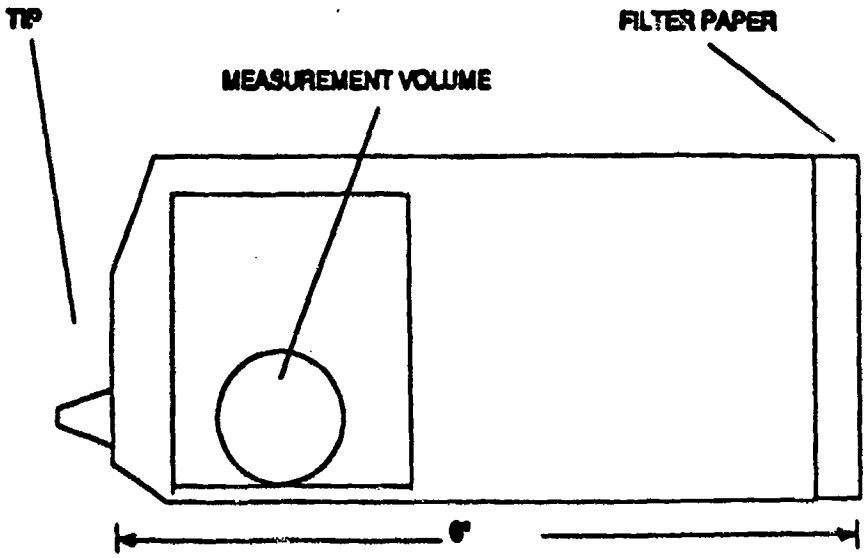

Figure 2.3 Origional Combined Optical and Collection Probe

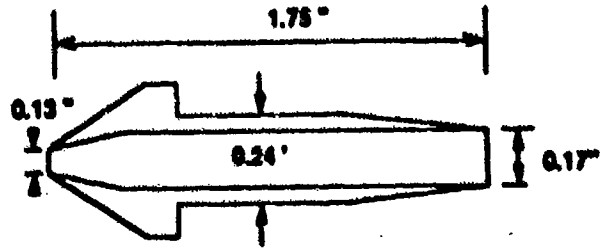

Figure 2.4 Cutaway View Of Probe Tip Interior

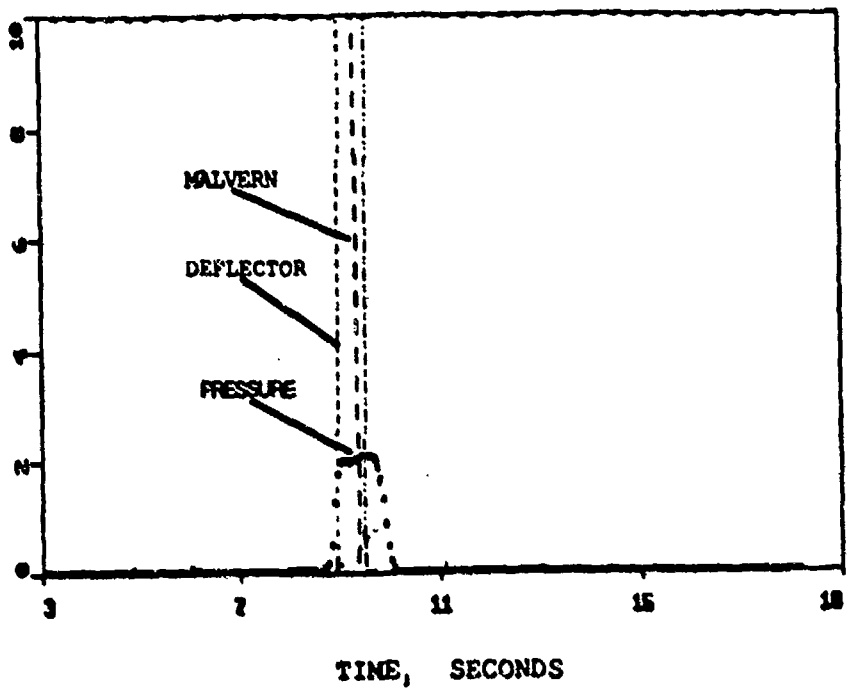

Figure 2.5 Firing Sequence and Pressure Time Trace

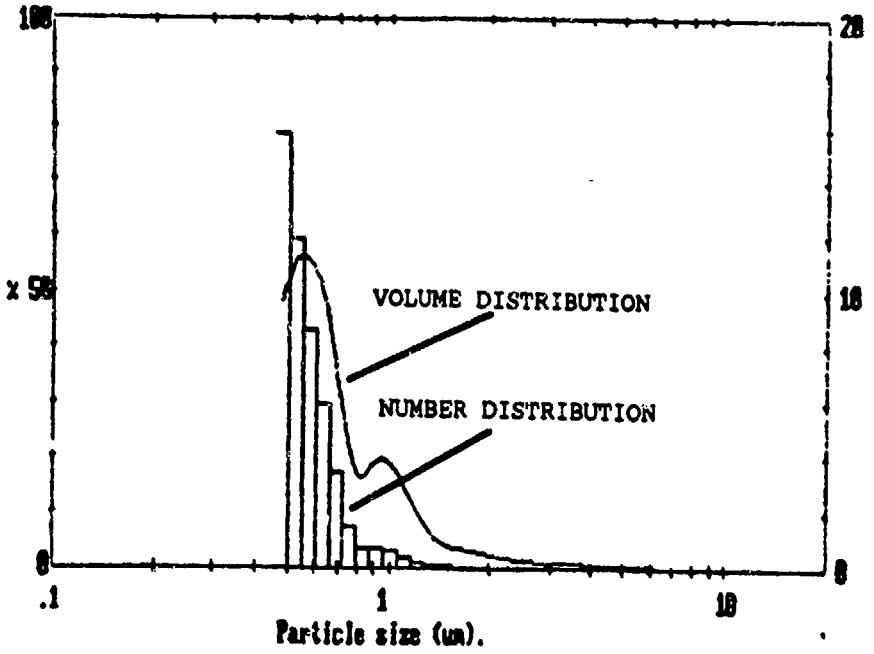

Figure 4.1 Run 12 Particle Size Volume/Number Distribution

Upper	in	Lower	Under	Upper	in	Lower	Under	Upper	in	Lower	Under	Span 1.14
				39.1	0.0	32.3	100	3.95	0.0	3.27	100	
				32.3	0.0	26.7	100	3.27	0.1	2.70	99.9	D[4,3] 0.67µm
				26.7	0.0	22.0	100	2.70	0.2	2.23	99.7	
				22.0	0.0	18.2	100	2.23	0.5	1.84	99.1	
180	0.0	149	100	18.2	0.0	15.1	100	1.84	1.4	1.52	97.8	D[3,2] 0.53µm
149	0.0	123	100	15.1	0.0	12.4	100	1.52	2.7	1.26	95.1	
123	0.0	102	100	12.4	0.0	10.3	100	1.26	7.5	1.04	87.6	
102	0.0	83.9	100	10.3	0.0	8.48	100	1.04	11.0	0.86	76.6	D[v,0.9] 1.09µm
83.9	0.0	69.3	100	8.48	0.0	7.01	100	0.86	11.1	0.71	65.5	
69.3	0.0	57.3	100	7.01	0.0	5.79	100	0.71	18.0	0.59	47.5	
57.3	0.0	47.3	100	5.79	0.0	4.79	100	0.59	22.0	0.48	25.5	D[v,0.1] 0.40µm
47.3	0.0	39.1	100	4.79	0.0	3.95	100	0.48	25.5	0.20	0.0	
Source = Data:Input				Beam length = 11.6 mm				Model indp				
				Residual = 1.344 %								D[v,0.5] 0.60µm
Focal length = 100 mm				Obscuration = 0.6958				Volume Conc. = 0.0011%				
Presentation = 2000				Volume distribution				Sp.S.A 11.2198 m²/cc.				

Figure 4.2 Run 12 Volume Distribution Percentage in Range

Upper	in	Lower	Under	Upper	in	Lower	Under	Upper	in	Lower	Under	Span 1.14
				39.1	0.0	32.3	100	3.95	0.0	3.27	100	
				32.3	0.0	26.7	100	3.27	0.0	2.70	100	D[4,3] 0.67µm
				26.7	0.0	22.0	100	2.70	0.0	2.23	100	
				22.0	0.0	18.2	100	2.23	0.0	1.84	100	
180	0.0	149	100	18.2	0.0	15.1	100	1.84	0.0	1.52	100	D[3,2] 0.53µm
149	0.0	123	100	15.1	0.0	12.4	100	1.52	0.1	1.26	99.9	
123	0.0	102	100	12.4	0.0	10.3	100	1.26	0.4	1.04	99.4	
102	0.0	83.9	100	10.3	0.0	8.48	100	1.04	1.2	0.86	98.3	D[v,0.9] 1.09µm
83.9	0.0	69.3	100	8.48	0.0	7.01	100	0.86	2.1	0.71	96.2	
69.3	0.0	57.3	100	7.01	0.0	5.79	100	0.71	6.0	0.59	90.2	
57.3	0.0	47.3	100	5.79	0.0	4.79	100	0.59	13.1	0.48	77.1	D[v,0.1] 0.40µm
47.3	0.0	39.1	100	4.79	0.0	3.95	100	0.48	77.1	0.20	0.0	
Source = Data:Input				Beam length = 11.6 mm				Model indp				D[v,0.5] 0.60µm
Focal length = 100 mm				Residual = 1.344 %								
Presentation = 2000				Obscuration = 0.6958				Volume Conc. = 0.0011%				
				Number distribution				Sp.S.A 11.2198 m²/cc.				

Figure 4.3 Run 12 Dumber Distribution Percentage In Range

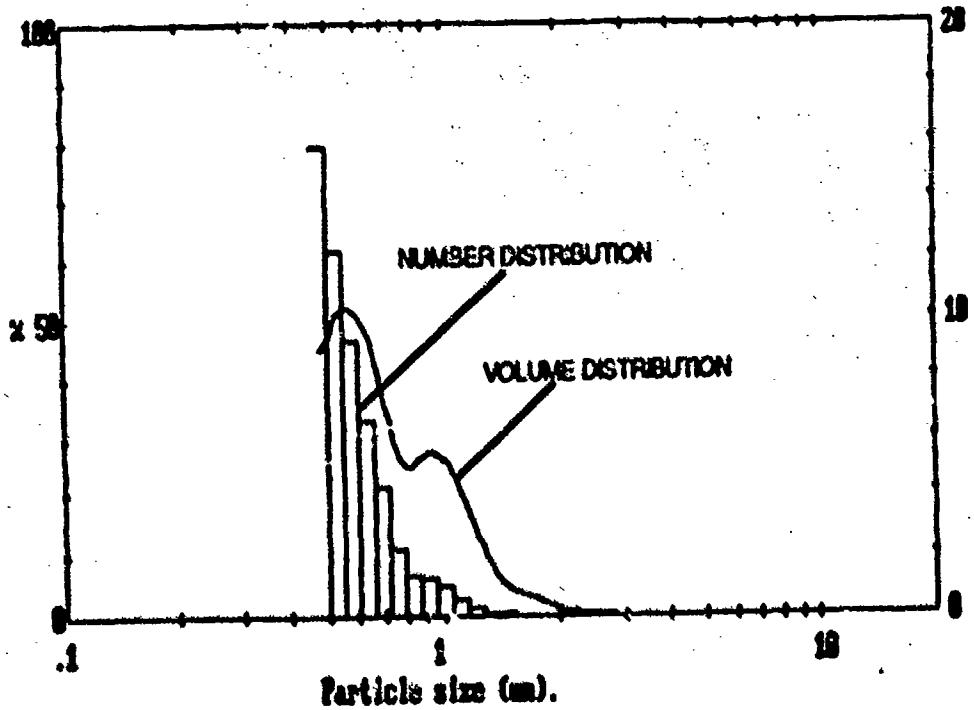

Figure 4.4 Run 13 Particle Size Volume/Number Distribution

Upper	in	Lower	Under	Upper	in	Lower	Under	Upper	in	Lower	Under	Span 1.26
				39.1	0.0	32.3	100	3.95	0.3	3.27	99.2	
				32.3	0.0	26.7	100	3.27	0.4	2.70	98.7	D[4,3] 0.68µm
				26.7	0.0	22.0	100	2.70	0.6	2.23	98.2	
				22.0	0.0	18.2	100	2.23	0.9	1.84	97.3	
180	0.0	149	100	18.2	0.0	15.1	100	1.84	1.4	1.52	95.9	D[3,2] 0.51µm
149	0.0	123	100	15.1	0.0	12.4	100	1.52	2.1	1.26	93.8	
123	0.0	102	100	12.4	0.0	10.3	100	1.26	5.1	1.04	88.6	
102	0.0	83.9	100	10.3	0.0	8.48	100	1.04	7.8	0.86	80.8	D[v,0.9] 1.08µm
83.9	0.0	69.3	100	8.48	0.1	7.01	99.9	0.86	8.2	0.71	72.7	
69.3	0.0	57.3	100	7.01	0.1	5.79	99.8	0.71	18.1	0.59	54.6	
57.3	0.0	47.3	100	5.79	0.1	4.79	99.7	0.59	24.2	0.48	30.4	D[v,0.1] 0.37µm
47.3	0.0	39.1	100	4.79	0.2	3.95	99.5	0.48	30.4	0.20	0.0	
Source = Data:Input				Beam length = 11.6 m				Model indp				D[v,0.5] 0.57µm
Focal length = 100 mm				Residual = 3.116 %								
Presentation = 2000				Obscuration = 0.7393				Volume Conc. = 0.0012%				
				Volume distribution				Sp.S.A 11.8790 m²/cc.				

Figure 4.5 Run 13 Volume Distribution Percentage In Range

Upper	in	Lower	Under	Upper	in	Lower	Under	Upper	in	Lower	Under	Span 1.26
				39.1	0.0	32.3	100	3.95	0.0	3.27	100	
				32.3	0.0	26.7	100	3.27	0.0	2.70	100	D[4,3] 0.68µm
				26.7	0.0	22.0	100	2.70	0.0	2.23	100	
				22.0	0.0	18.2	100	2.23	0.0	1.84	100	
180	0.0	149	100	18.2	0.0	15.1	100	1.84	0.0	1.52	100	D[3,2] 0.51µm
149	0.0	123	100	15.1	0.0	12.4	100	1.52	0.1	1.26	99.9	
123	0.0	102	100	12.4	0.0	10.3	100	1.26	0.3	1.04	99.6	
102	0.0	83.9	100	10.3	0.0	8.48	100	1.04	0.7	0.86	98.9	D[v,0.9] 1.08µm
83.9	0.0	69.3	100	8.48	0.0	7.01	100	0.86	1.3	0.71	97.6	
69.3	0.0	57.3	100	7.01	0.0	5.79	100	0.71	5.2	0.59	92.4	
57.3	0.0	47.3	100	5.79	0.0	4.79	100	0.59	12.6	0.48	79.8	D[v,0.1] 0.37µm
47.3	0.0	39.1	100	4.79	0.0	3.95	100	0.48	79.8	0.20	0.0	
Source = Data:Input				Beam length = 11.6 m				Model indp				D[v,0.5] 0.57µm
Focal length = 100 mm				Residual = 3.116 %								
Presentation = 2000				Obscuration = 0.7393				Volume Conc. = 0.0012%				
				Number distribution				Sp.S.A 11.8790 m²/cc.				

Figure 4.6 Run 13 Number Distribution Percentage In Range

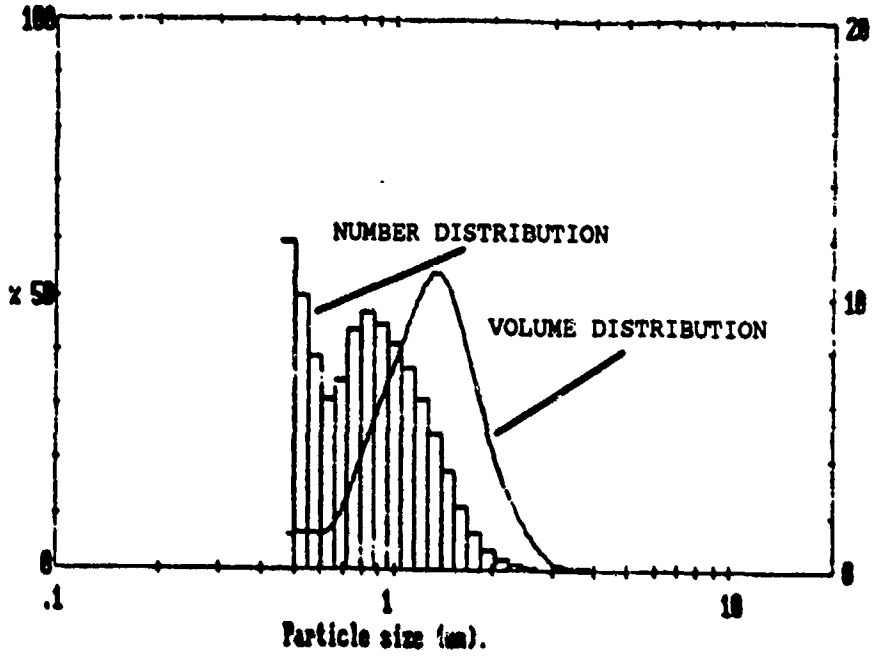

Figure 4.7 Run 14 Particle Size Volume/Number Distribution

Upper	in	Lower	Under	Upper	in	Lower	Under	Upper	in	Lower	Under	Span 0.94
				39.1	0.0	32.3	100	3.95	0.2	3.27	99.8	
				32.3	0.0	26.7	100	3.27	0.8	2.70	99.0	D[4,3] 1.31µm
				26.7	0.0	22.0	100	2.70	3.4	2.23	95.6	
				22.0	0.0	18.2	100	2.23	8.4	1.84	87.2	
180	0.0	149	100	18.2	0.0	15.1	100	1.84	16.3	1.52	71.0	D[3,2] 1.09µm
149	0.0	123	100	15.1	0.0	12.4	100	1.52	21.3	1.26	46.6	
123	0.0	102	100	12.4	0.0	10.3	100	1.26	19.3	1.04	30.3	
102	0.0	83.9	100	10.3	0.0	8.48	100	1.04	13.6	0.86	16.7	D[v,0.9] 1.93µm
83.9	0.0	69.3	100	8.48	0.0	7.01	100	0.86	7.9	0.71	8.8	
69.3	0.0	57.3	100	7.01	0.0	5.79	100	0.71	3.1	0.59	5.7	
57.3	0.0	47.3	100	5.79	0.0	4.79	100	0.59	2.9	0.48	2.7	D[v,0.1] 0.74µm
47.3	0.0	39.1	100	4.79	0.0	3.95	100	0.48	2.7	0.20	0.0	
Source = Data:Input				Mean length = 11.6 us				Model indp				D[v,0.5] 1.26µm
				Residual = 0.937 %								
Focal length = 100 mm				Obscuration = 0.7465				Volume Conc. = 0.00331%				
Presentation = 2000				Volume distribution				Sp.S.A 5.4926 m²/cc.				

Figure 4.8 Run 14 Volume Distribution Percentage In Range

Upper	in	Lower	Under	Upper	in	Lower	Under	Upper	in	Lower	Under	Span 0.94
				39.1	0.0	32.3	100	3.95	0.0	3.27	100	
				32.3	0.0	26.7	100	3.27	0.0	2.70	100	D[4,3] 1.31µm
				26.7	0.0	22.0	100	2.70	0.1	2.23	99.9	
				22.0	0.0	18.2	100	2.23	0.6	1.84	99.3	
180	0.0	149	100	18.2	0.0	15.1	100	1.84	1.9	1.52	97.4	D[3,2] 1.09µm
149	0.0	123	100	15.1	0.0	12.4	100	1.52	4.4	1.26	92.9	
123	0.0	102	100	12.4	0.0	10.3	100	1.26	7.1	1.04	85.8	
102	0.0	83.9	100	10.3	0.0	8.48	100	1.04	8.9	0.86	77.0	D[v,0.9] 1.93µm
83.9	0.0	69.3	100	8.48	0.0	7.01	100	0.86	9.1	0.71	67.8	
69.3	0.0	57.3	100	7.01	0.0	5.79	100	0.71	6.4	0.59	61.5	
57.3	0.0	47.3	100	5.79	0.0	4.79	100	0.59	10.7	0.48	50.8	D[v,0.1] 0.74µm
47.3	0.0	39.1	100	4.79	0.0	3.95	100	0.48	50.8	0.20	0.0	
Source = Data:Input				Beam length = 11.6 mm				Model indp				D[v,0.5] 1.26µm
				Residual = 0.937 %								
Focal length = 100 mm				Obscuration = 0.7465				Volume Conc. = 0.0033%				
Presentation = 2000				Number distribution				Sp.S.A 5.4926 m²/cc.				

Figure 4.9 Run 14 Number Distribution Percentage In Range

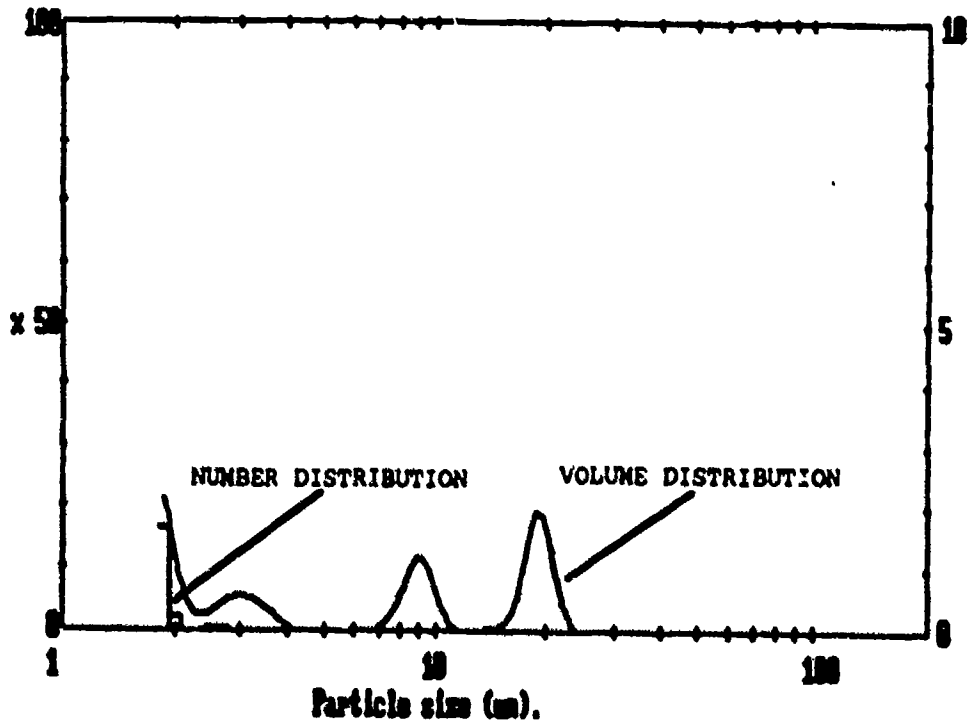

Figure 4.10 Run 15 Particle Size Volume/Number Distribution

Upper	in	Lower	Under	Upper	in	Lower	Under	Upper	in	Lower	Under	Span 2.63
				57.7	0.0	49.8	100	9.82	2.3	8.47	91.3	
				49.8	0.0	43.0	100	8.47	1.0	7.30	90.4	D[4,3] 2.42µm
				43.0	0.0	37.0	100	7.30	0.0	6.30	90.3	
				37.0	0.0	32.0	100	6.30	0.0	5.43	90.3	
188	0.0	162	100	32.0	0.0	27.5	100	5.43	0.0	4.68	90.3	D[3,2] 1.12µm
162	0.0	140	100	27.5	0.0	23.8	100	4.68	0.0	4.05	90.3	
140	0.0	121	100	23.8	0.9	20.5	99.1	4.05	0.5	3.48	89.8	
121	0.0	104	100	20.5	3.7	17.7	95.3	3.48	1.0	3.02	88.8	D[v,0.9] 3.61µm
104	0.0	89.8	100	17.7	1.1	15.3	94.3	3.02	1.0	2.60	87.8	
89.8	0.0	77.5	100	15.3	0.1	13.2	94.2	2.60	0.6	2.23	87.2	
77.5	0.0	66.8	100	13.2	0.0	11.4	94.2	2.23	1.6	1.93	85.6	D[v,0.1] 0.68µm
66.8	0.0	57.7	100	11.4	0.6	9.82	93.6	1.93	85.6	0.50	0.0	
Source = Data:Input Focal length = 100 mm Presentation = pia				Beam length = 25.0 mm Log. Diff. = 3.212 Obscuration = 0.6023 Volume distribution				Model indp Volume Conc. = 0.0014% Sp.S.A 5.3779 m²/cc.				D[v,0.5] 1.11µm

Figure 4.11 Run 15 Volume Distribution Percentage In Range

Upper	in	Lower	Under	Upper	in	Lower	Under	Upper	in	Lower	Under	Span 2.63
				57.7	0.0	49.8	100	9.82	0.0	8.47	100	
				49.8	0.0	43.0	100	8.47	0.0	7.30	100	D[4,3] 2.42µm
				43.0	0.0	37.0	100	7.30	0.0	6.30	100	
				37.0	0.0	32.0	100	6.30	0.0	5.43	100	
188	0.0	162	100	32.0	0.0	27.5	100	5.43	0.0	4.68	100	D[3,2] 1.12µm
162	0.0	140	100	27.5	0.0	23.8	100	4.68	0.0	4.05	100	
140	0.0	121	100	23.8	0.0	20.5	100	4.05	0.0	3.48	100	
121	0.0	104	100	20.5	0.0	17.7	100	3.48	0.0	3.02	100	D[v,0.9] 3.61µm
104	0.0	89.8	100	17.7	0.0	15.3	100	3.02	0.1	2.60	99.9	
89.8	0.0	77.5	100	15.3	0.0	13.2	100	2.60	0.0	2.23	99.8	
77.5	0.0	66.8	100	13.2	0.0	11.4	100	2.23	0.2	1.93	99.7	D[v,0.1] 0.68µm
66.8	0.0	57.7	100	11.4	0.0	9.82	100	1.93	99.7	0.50	0.0	
Source = Data:Input Focal length = 100 mm Presentation = pia				Beam length = 25.0 mm Log. Diff. = 1.212 Obscuration = 0.6023 Number distribution				Model indp Volume Conc. = 0.0014% Sp.S.A 5.3779 m²/cc.				D[v,0.5] 1.11µm

Figure 4.12 Run 15 Number Distribution Percentage In Range

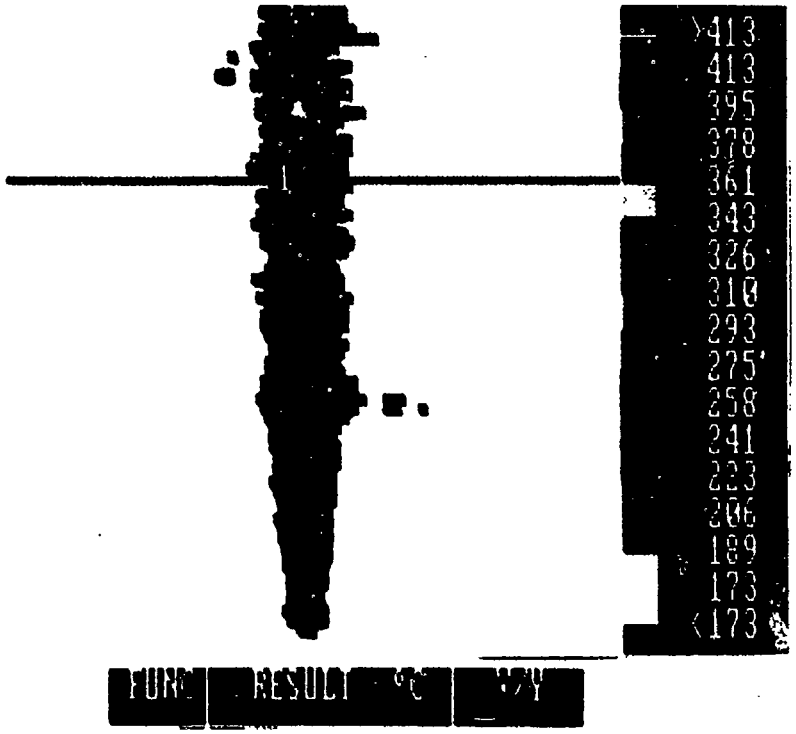

Figure 4.13 IR Image Of Plume For Run 15

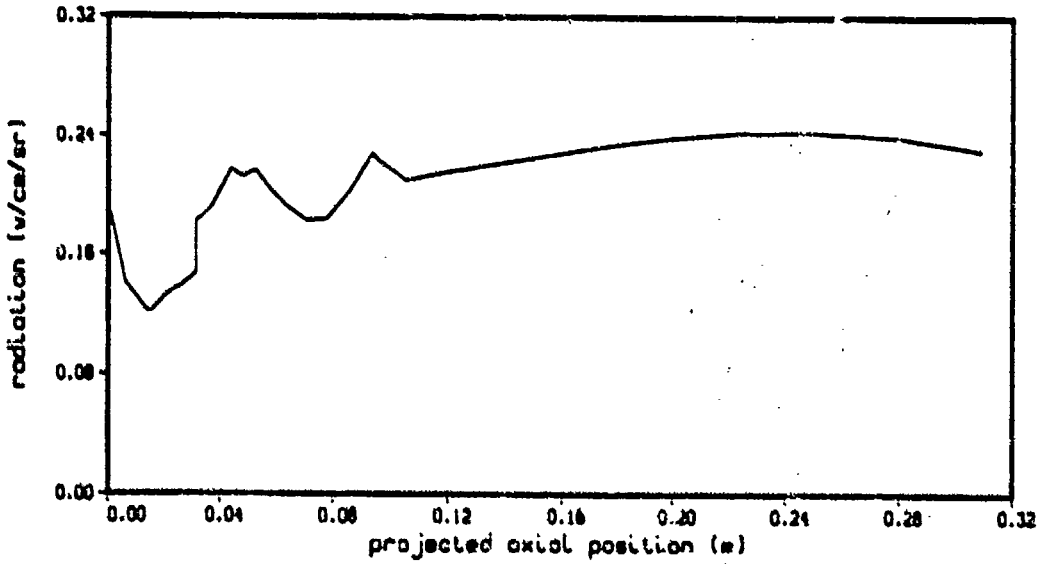

Figure 4.14 Predicted Radiation vs. Axial Position For Propellant DD1 Burned In Subscale Motor At 600 Psia, 4.2-4.5μ

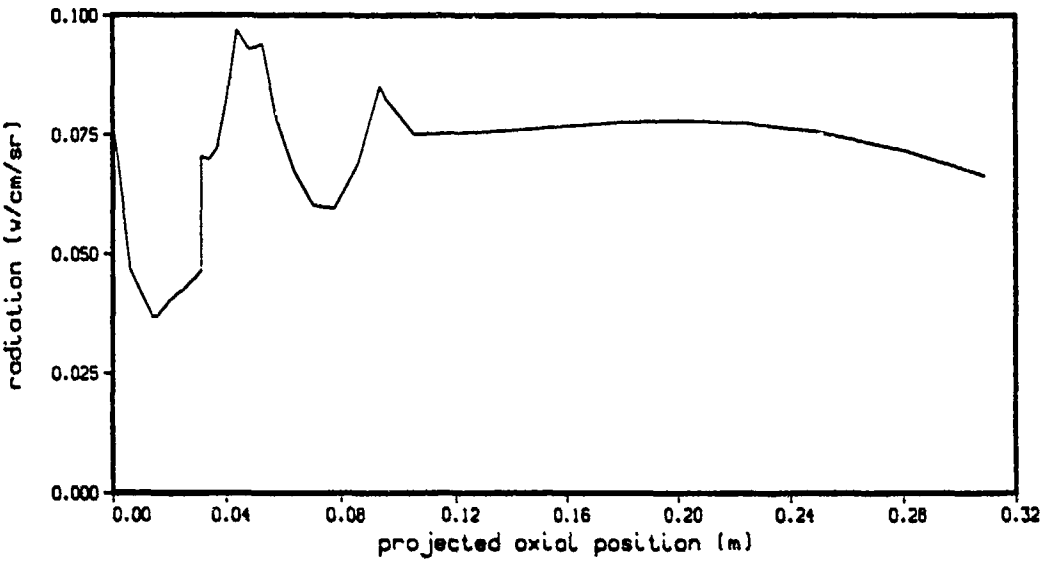

Figure 4.15 Predicted Radiation vs. Axial Position For Propellant DD1 Burned In Subscale Motor At 600 Psia, 2.6-3.0μ

APPENDIX C

MICROPEP OUTPUT

```
ALUMINUM (PURE CRYSTALINE)        0 0.09760   1AL
AMMONIUM PERCHLORATE (AP)      -602 0.07040   1CL 4H  1N  4O
FERRIC OXIDE HEMATITE         -1235 0.18480   2FE 3O
HTPB/CURATIVE (JOS)              -5 0.03290 656C 978H  5N 13O

INGREDIENT WEIGHTS (IN ORDER) AND TOTAL WEIGHT (LAST ITEM IN LIST)

  16.0000   70.0000    0.2000   13.8000  100.0000

THE PROPELLANT DENSITY IS 0.06334 LB/CU-IN OR  1.7532 GM/CC

NUMBER OF GRAM ATOMS OF EACH ELEMENT PRESENT IN INGREDIENTS

  3.859172 H    0.990126 C    0.603307 N    2.406418 O
  0.593032 AL   0.595760 CL   0.002505 FE

**********CHAMBER RESULTS FOLLOW**********

 T(K) T(F) P(ATM)  P(PSI) ENTHALPY ENTROPY  CP/CV  SGAMMA   RT/V
3286. 5456.  21.43  315.00  -42.46  237.48 1.1807 1.1355   5.866  TCRE

DAMPED AND UNDAMPED SPEED OF SOUND= 2982.003 AND 3561.320 FT/SEC

SPECIFIC HEAT (MOLAR) OF GAS AND TOTAL=   9.456  12.057
NUMBER MOLS GAS AND CONDENSED=  3.6528  0.2799

 1.10161 H2      0.93751 CO      0.51220 HCl     0.47968 H2O
 0.30071 N2      0.27990 Al2O3*  0.15305 H       0.05251 CO2
 0.04754 Cl      0.02774 HO      0.01827 AlCl    0.00557 AlOCl
4.16E-03 AlCl2   2.26E-03 O      1.89E-03 AlHO2  1.81E-03 NO
1.43E-03 AlHO    1.19E-03 FeCl2  1.14E-03 Fe     7.22E-04 AlO
4.29E-04 Al      3.98E-04 AlCl3  3.90E-04 O2     1.35E-04 Al2O
8.60E-05 FeCl    6.28E-05 FeO    5.91E-05 Cl2    5.48E-05 AlH
4.90E-05 CHO     2.22E-05 NH3    2.09E-05 COCl   1.86E-05 OCl
1.75E-05 FeH2O2  1.70E-05 N      1.53E-05 HOCl   1.36E-05 Al2O2
1.28E-05 CNH     1.09E-05 NH2    6.63E-06 NH     5.26E-06 AlO2
3.39E-06 CH2O    3.06E-06 HO2    2.17E-06 NHO    1.19E-06 AlHO
9.38E-07 CNHO    5.82E-07 FeCl3  2.83E-07 CN

THE MOLECULAR WEIGHT OF THE MIXTURE IS  25.427

TOTAL HEAT CONTENT (298 REF)  =1347.500 CAL/GM
SENSIBLE HEAT CONTENT (298 REF)=1260.668 CAL/GM
```

**********EXHAUST RESULTS FOLLOW**********

T(K)	T(F)	P(ATM)	P(PSI)	ENTHALPY	ENTROPY	CP/CV	SGAMMA	RT/V
2330.	3735.	1.09	16.00	-101.97	237.48	1.1791	1.1599	0.308 TCRE

DAMPED AND UNDAMPED SPEED OF SOUND= 2435.821 AND 2948.325 FT/SEC

SPECIFIC HEAT (MOLAR) OF GAS AND TOTAL= 9.228 12.070
NUMBER MOLS GAS AND CONDENSED= 3.5353 0.2962

1.16545 H2	0.92533 CO	0.58241 HCl	0.46114 H2O
0.30162 N2	0.29621 Al2O3*	0.06477 CO2	0.02203 H
7.87E-03 Cl	2.32E-03 FeCl2	1.49E-03 HO	2.82E-04 AlCl
1.62E-04 Fe	1.27E-04 AlOCl	1.16E-04 AlCl2	5.25E-05 AlCl3
4.18E-05 NO	2.02E-05 AlHO2	1.88E-05 O	1.26E-05 AlHO
9.41E-06 FeCl	4.00E-06 Cl2	3.11E-06 O2	3.07E-06 FeH2O2
2.75E-06 NH3	2.53E-06 FeO	1.14E-06 CHO	7.27E-07 CNH
5.70E-07 COCl	5.54E-07 AlO	3.70E-07 FeCl3	3.38E-07 Al
2.82E-07 HOCl			

THE MOLECULAR WEIGHT OF THE MIXTURE IS 26.099

TOTAL HEAT CONTENT (298 REF) = 865.745 CAL/GM
SENSIBLE HEAT CONTENT (298 REF)= 814.974 CAL/GM

*****PERFORMANCE: FROZEN ON FIRST LINE, SHIFTING ON SECOND LINE******

An exact method for determining throat conditions was used
The frozen & shifting STATE gammas for the throat are: 1.1794 1.1371
ISentropic EXponent shown below is the gamma for the chamber to throat PROCESS.

IMPULSE	IS EX	T*	P*	C*	ISP*	OPT EX	D-ISP	A*M.	EX T	ADH
222.6	1.1814	3024.	12.46	5084.8		3.65	390.2	0.50183	2063.	499239.
227.6	1.1361	3103.	12.36	5155.1	197.6	3.85	399.0	0.50877	2330.	568988.

REFERENCES

1. Dash, S.M., Analysis of Exhaust Plumes and Their Interaction with Missile Airframes in Tactical Missiles Aerodynamics, Vol 104, American Institute of Aeronautics and Astronautics, Inc (AIAA), 1986.

2. Nelson, H.F., Influence of Particulates on Infrared Emission from Tactical Rocket Exhausts, Vol 21, No 5, Sept-Oct 1984, American Institute of Aeronautics and Astronautics, Inc., 1984.

3. Dash, S.M., et.al., Prediction of Rocket Plume Flowfields for Infrared Signature Studies, J. Spacecraft, Vol 17, No 3, May-June 1980, pp.190-199.

4. Kim, H., Multiple-Wavelength Transmission Measurements in Rocket Motor Plumes, Master's Thesis, Naval Postgraduate School, Monterey, California, September 1991.

5. Eno, T.J., A Combined Optical and Collection Probe for Solid Propellant Exhaust Analysis, Master's Thesis, Naval Postgraduate School, Monterey, California, December 1989.

6. Kellman, L.J., Modification and Experimental Validation of a Combined Optical and Collection Probe for Solid Propellant Exhaust Analysis, Master's Thesis, Naval Postgraduate School, Monterey. California, March 1991.

7. Youngborg, E.D., Pruitt, T.E., Smith, M.J., and Netzer, D.W., Light-diffraction Particle Size Measurements in Small Solid-Propellant Rockets, Vol 26, No 3, May-June 1990, American Institute of Aeronautics and Astronautics, Inc. (AIAA), 1990.

8. *Mastersizer Instruction Manual*, Malvern Instruments LTD, Manual Version IM 100, Issue 3, October 1989, pp. 1.23-1.26.

9. *Malvern 2600HSD Instruction Manual*, Malvern Instruments LTD.

10. Thermovision 870 Operating Manual, AGEMA Infrared Systems AB, 1986.

11. Gulder, O.L., Multiple Scattering Effects in Droplet Sizing of Dense Fuel Sprays by Laser Diffraction, NATO AGARD Conference Proceedings, No 422, Combustion and Fuels in Gas Turbine Engines, June 1988.

INITIAL DISTRIBUTION LIST

1.	Defense Technical Information Center Cameron Station Alexandria, VA 22304-6145	2
2.	Library, Code 0142 Naval Postgraduate School Monterey, CA 93943-5100	2
3.	Chairman, Code AA/Co Department of Aeronautics and Astronautics Naval Postgraduate School Monterey, CA 93943-5100	1
4.	Department of Aeronautics and Astronautics Attn: Prof. Netzer (Code AA/NT) Monterey, CA 93943-5100	2
5.	Department of Aeronautics and Astronautics Attn: Dr. Laredo (Code AA/NT) Monterey, CA 93943-5100	1
6.	Lt John A. Racine 127 Sikes Dr Crestview, FL 32536	2